Gap solitons and nonlinear Bloch states in Bose-Einstein condensates with current-dependent interactions

Jintao Xu, Qian Jia, and Haibo Qiu [*]

School of Science, Xi'an University of Posts and Telecommunications, Xi'an 710121, China

Antonio Muñoz Mateo [†]

Departamento de Física, Universidad de La Laguna, La Laguna, Tenerife 38200, Spain

We show how the chiral properties of Bose-Einstein condensates subject to current-density interactions and loaded in optical lattices can be observed in the realization of nonlinear Bloch states, whose spectrum lacks the usual periodic structure. Chirality is also manifested by spatially localized states, or gap solitons, which are found for positive rotation rates of the lattice at the energy gaps between the linear energy bands, whereas for negative rotations they appear in the semi-infinite gap of the linear spectrum. The stability of extended and localized states is checked through the spectrum of linear excitations and nonlinear time evolution of perturbed states, and the phenomenon of Bloch oscillations is explored. Our results are obtained in quasi-one-dimensional ring geometries with feasible experimental parameters.

I. INTRODUCTION

Synthetic gauge fields that depend locally on the density of matter have been recently realized in ultracold-atom settings [1–4]. The unusual properties of these systems were theoretically predicted by means of a nonlocal unitary transformation that maps the density-dependent gauge into a current-dependent interaction [5,6]. Bose-Einstein condensates (BECs) endowed with such interparticle interactions were shown to exhibit chiral properties in a free expansion, the onset of persistent currents, or the center-of-mass oscillations [7,8]; additionally, in the absence of external potential, it was demonstrated that chiral bright solitons can exist only if they move along one (but not the opposite) direction [4,5,9,10], and that collisions between them differ significantly from those between regular solitons [11,12].

Many aspects of this chiral theory remain unexplored, and very recent experimental realizations [4] open new prospects for testing the theoretical predictions. A significant subject that was previously restricted to solid-state systems, the matter dynamics in periodic potentials, became also accessible to the field of ultracold gases with the realization of optical lattices [13,14]. As far as we know, this subject has still not been addressed within the chiral theory.

In this paper, we focus on BECs that are loaded in optical lattices and subject to interactions that depend locally on the current density. The lattice is assumed to be imprinted on a quasi-one-dimensional (1D) ring, as generated by a tight transverse confinement of the atoms, and to be able to rotate. In particular, within the framework of a generalized

Gross-Pitaevskii equation, we study the properties of nonlinear Bloch waves and gap solitons, and demonstrate their unusual properties. While the energy dispersion of the former states loses the usual periodic structure, and new nonregular Bloch states emerge, the situation of gap solitons within the energy gaps changes drastically with the direction of the rotation rate. We analyze the spectrum of linear excitations and show that the stability of both extended and localized states is also conditioned by the chiral properties. Finally, we perform numerical simulations of the equation of motion to explore the stability of stationary states against small perturbations, and also the existence of Bloch oscillations in the presence of current-density interactions.

II. MODEL

We assume that the condensate wave function $\psi(x, t)$ follows a generalized Gross-Pitaevskii equation in a ring of radius R:

$$i\hbar \frac{\partial \psi}{\partial t} = \left[\frac{(-i\hbar\partial_x - m\Omega R)^2}{2m} + U_{\text{latt}} + \hbar\kappa J \right] \psi, \quad (1)$$

where $U_{\text{latt}}(x) = U_0 \sin^2(\pi x/d)$ is the lattice potential, with amplitude U_0 and lattice spacing d, which can rotate with angular velocity Ω. The strength of the current-dependent mean field is measured by the dimensionless parameter κ, and $J(x, t) = \hbar(\psi^*\partial_x\psi - \psi\partial_x\psi^*)/(i2m)$ is the current density in the laboratory frame. The total number of particles $N = \int dx|\psi|^2$, and the total energy (which does not include an explicit dependency on the current density)

$$E = \int dx\, \psi^* \left[\frac{(-i\hbar\partial_x - m\Omega R)^2}{2m} + U_{\text{latt}} \right] \psi, \quad (2)$$

[*]phyqiu@gmail.com
[†]ammateo@ull.edu.es

are conserved quantities [5]. We particularize our analysis on an M-site lattice over the ring, so that $2\pi R = M d$. As energy reference, we will make use of the lattice recoil energy $E_L = \hbar^2(\pi/d)^2/(2m)$ [13].

The stationary states take the form $\psi(x,t) = \psi(x) \exp(-i\mu t/\hbar)$, with μ as the energy eigenvalue. In the search for stationary states, it is worth noticing that, from the continuity equation $\partial_t |\psi|^2 + \partial_x (J - |\psi|^2 \Omega R) = 0$, the current density fulfills $J - |\psi|^2 \Omega R = J_0$, where J_0 is a constant, thus it transforms the equation of motion (1) into the regular time-independent Gross-Pitaevskii equation

$$(\mu - \hbar\kappa J_0)\psi = \left[\frac{(-i\hbar\partial_x - m\Omega R)^2}{2m} + U_{\text{latt}} + g_\Omega |\psi|^2 \right]\psi, \tag{3}$$

where the effective constant-interaction strength is $g_\Omega = \hbar\kappa\Omega R$. Furthermore, if the lattice does not rotate, the initial nonlinear equation (1) is transformed into the time-independent Schrödinger equation

$$(\mu - \hbar\kappa J_0)\psi = \left[-\frac{\hbar^2}{2m}\partial_x^2 + U_{\text{latt}} \right]\psi, \tag{4}$$

with the current constraint $J_0 = |\psi(x)|^2 \hbar\partial_x\theta(x)/m$, where $\theta = \arg \psi(x)$ is the phase.

The linear excitations $\delta\psi_j = [u_j, v_j]^T$ of stationary states $\psi(x,t) \to \exp(-i\mu t/\hbar)\{\psi(x) + \sum_j[u_j(x) \exp(-i\omega_j t) + v_j(x)^* \exp(i\omega_j^* t)]\}$, with j being a mode index, can be obtained through the Bogoliubov equation $B\delta\psi_j = \hbar\omega_j \delta\psi_j$. The Bogoliubov matrix is given by

$$B = \begin{pmatrix} H_{\text{GP}} + i\kappa B_{uu} - \mu & i\kappa B_{uv} \\ i\kappa B_{uv}^* & -H_{\text{GP}}^* + i\kappa B_{uu}^* + \mu \end{pmatrix}, \tag{5}$$

where $H_{\text{GP}} = (-i\hbar\partial_x - m\Omega R)^2/2m + U_{\text{latt}} + \hbar\kappa J$ is the Hamiltonian operator in Eq. (1), $B_{uu} = \hbar^2(\psi \partial_x \psi^* - |\psi|^2\partial_x)/2m$, and $B_{uv} = -\hbar^2(\psi \partial_x \psi - \psi^2\partial_x)/2m$. Linear excitations with complex frequencies, $\text{Im}(\omega_j) \neq 0$, lead to the exponential growth (in the linear regime) of small perturbations on the stationary state that can produce its decay during time evolution.

III. EXTENDED AND LOCALIZED EIGENSTATES

In a nonrotating linear system ($\Omega = 0$ and $\kappa = 0$), the dispersion relations of quantum states in a ring lattice consist of energy bands separated by energy gaps [15]. The corresponding spectrum of eigenstates can be described in terms of Bloch waves $\psi_{n,k}(x,t) = \exp[i(kx - \epsilon_{n,k}t/\hbar)] u_{n,k}(x)$, with eigenenergies $\epsilon_{n,k}$, where $n = 1, 2, \ldots$ identifies the band number, and $k = q k_0$, with $q = 0, \pm 1, \pm 2, \ldots$ and $k_0 = 1/R$, is the wave number associated with the quasimomentum $\hbar k$. The functions $u_{n,k}(x)$ share spatial period with the lattice $u_{n,k}(x + d) = u_{n,k}(x)$, so that the probability density profile is homogeneous over the lattice sites. If the lattice is finite, and contains M sites, there are just M values of quasimomentum [15].

In a system with varying contact interactions, the linear Bloch waves have been shown to find continuation as nonlinear Bloch waves when the interactions are switched on [13,16]. We will show that this continuation also exists

in the presence of current-density interactions. In addition, differently to the case of contact interactions, there exist new extended states with a nonhomogeneous density profile over the lattice sites.

A. Nonlinear Bloch waves

First, we focus on the dispersion of the system at $\Omega = 0$ for varying quasimomentum. Insight can be obtained from the comparison with a system subject to contact interactions (hence following the usual GP equation); in this case, the linear energy bands are shifted to higher energies when the interaction is repulsive, whereas the opposite happens for attractive interaction. Therefore, in the presence of current-density interaction, where the effective interaction changes from repulsive to attractive according to the sign of the particle current, the resulting dispersion curves are expected to be asymmetric with respect to the value of quasimomentum, with energies higher than the linear bands for states with positive currents, and lower than the linear bands for states with negative currents.

As can be seen in Fig. 1(a), this is indeed the scenario shown by our numerical results for a ring lattice with $M = 10$ sites and shallow depth $s = 2$. The number of particles has been fixed for the nonlinear states considered to give $\kappa N/(2\pi R) = 0.47/d$; correspondingly, the order of magnitude of the nonlinearity in Eq. (3) is $g_\Omega N/(2\pi R) = 4.7(R/d)\hbar\Omega$. For comparison, contact interaction cases are represented, and have been parametrized by the nondimensional quantity $g = m d g_{1D}/\hbar^2$, where g_{1D} is the one-dimensional contact interaction strength, so that $|g| = \kappa$. The lowest-energy band of the linear system (dotted line) lays in between the lowest chemical potential bands of nonlinear systems with positive (open symbols joined by dashed lines to guide the eye) and negative (open symbols joined by dot-dashed lines) contact interactions, whereas the energy eigenvalues of the system with current-density interaction (filled symbols) vary as predicted. The states with minimum (zero) and maximum ($k = 5 k_0$) values of quasimomentum have no particle currents, thus they follow a linear (Schrödinger) equation of motion, and match the energy of the linear bands. Four instances of Bloch states, with quasimomentum wave number $k/k_0 = 0, 1, -1, 5$, represented by their density and phase profiles, are shown in Fig. 1(b).

B. Nonregular Bloch states

An interesting novelty of the systems with current-density interactions, contrary to the case of contact interactions, is the existence of extended stationary states that do not conform to the usual picture of Bloch states, since they present a nonhomogeneous density profile over the lattice sites. They do not conform either to the features of alternative states hosting dark solitons in the lattice [17]. We will refer to them as nonregular Bloch states, since the quasimomentum, associated with the phase winding number $q = k/k_0$, is still a well-defined quantity. As a general aspect, the higher the variation between density peaks of lattice sites that they present, the lower the constant current density becomes. Our numerical results for characteristic quantities suggest a continuum of
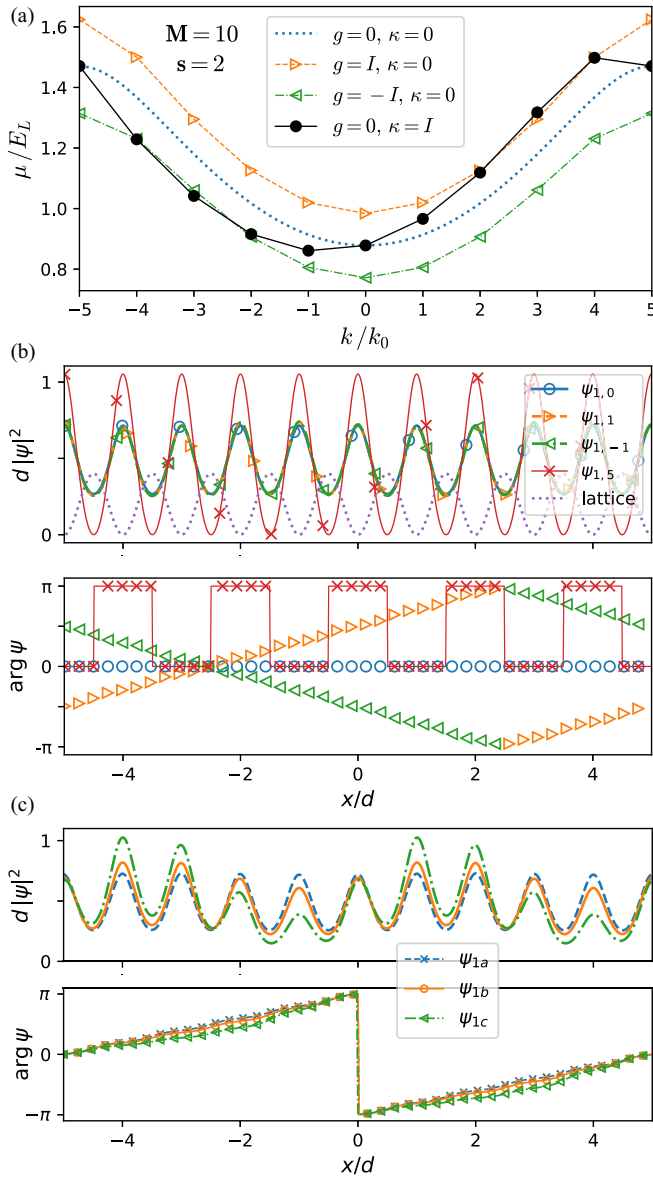
FIG. 1. (a) Linear (dotted line) and nonlinear (symbols) lowest-energy bands for a ring lattice at rest, $\Omega = 0$, with ten sites, $M = 10$, lattice depth $s = 2$, and average number density fixed by $\kappa N/(2\pi R) = 0.47/d$. Two types of interparticle interactions with equal strength are represented: contact interaction parametrized by $|g|$ (see text), both repulsive $g > 0$ and attractive $g < 0$, and current-dependent interaction κ, with $|g| = \kappa = 4.7/N$ (denoted by I in the legend). (b) Density (top) and phase (bottom) profiles of nonlinear Bloch states $\psi_{n,k}$ in the presence of current-density interactions, $\kappa \neq 0$ and $g = 0$. (c) Three instances of nonregular Bloch states with quasimomentum $k = k_0$, from almost homogenous, ψ_{1a}, to large variations, ψ_{1c}, in the density peaks.

nonregular Bloch states, for we were able to find close states with very small differences, of the order of 1‰ in energies. The linear Eq. (4) sheds light on this phenomenon, since it admits solutions as linear superpositions of states with the same eigenvalue $\mu - \hbar\kappa J_0$.

Figure 1(c) shows the density (top) and phase (bottom) profiles of three nonregular Bloch states with winding number

$q = k/k_0 = 1$. They range from almost homogeneous ψ_{1a}, to intermediate ψ_{1b}, and up to large variation ψ_{1c}, in the density peaks. The density modulation over the whole lattice has the form $n_k [1 + \beta \sin(k_0 x)]$, where n_k is the density of the homogenous Bloch state, and β varies from almost zero for ψ_{1a}, to $\beta = 0.6$ for ψ_{1c}. Despite the large differences in the density profile, their energy eigenvalues differ by less than 1%, and their energies differ by less than 1‰. The phase profiles show also small differences and follow a monotonic increase in the range $[0, 2\pi]$.

C. Lattice rotation and gap solitons

Gap solitons are localized states in systems loaded in optical lattices; they usually occupy a few sites, a small region of the whole lattice. Although their existence can be easily understood in systems with attractive interactions, similarly as in translation-invariant settings, their emergence in the presence of repulsive interactions is *a priori* not that evident [18], and can be explained through the sign change induced by the lattice in the effective mass of the particles (see for instance Ref. [19]). In this paper, the current-density interaction provides both possibilities for the emergence of gap solitons, which become distinct for positive and negative current densities. Since the interaction (or nonlinearity) is necessary for the solitons to exist, the ring lattice has to rotate in order for the gap solitons to emerge.

Although the finite lattice considered here, having M sites, allows for only M Bloch waves, the introduction of rotation gives access to the continuous spectrum of the infinite lattice [16]. In systems with Galilean symmetry (as happens for contact interactions), for varying rotation rate $\Omega \in (-M/2, M/2) \times \Omega_0$, where $\Omega_0 = \hbar/(mR^2)$, the energy of each Bloch wave $\epsilon_{n,k}(\Omega)$ in the finite lattice [as obtained from Eq. (2)] reproduces the energy band profile against quasimomentum in the first Brillouin zone $k \in (-\pi/d, \pi/d]$ of the infinite lattice with $\Omega = 0$. The dispersion graph, $\epsilon_{n,k}$ versus Ω, is also useful in understanding the emergence of gap solitons; the energy degeneracies found in this graph for the linear system, which correspond to crossings of Bloch-wave trajectories, provide the origin of gap solitons when the interparticle interactions are switched on. Thus, gap solitons are the nonlinear continuation of linear states made of Bloch-wave superpositions [16].

Figure 2 shows our numerical results for stationary states in a moving ring lattice with current density interactions and the same parameters as in Fig. 1. The eigenenergy (left) and current density (right) of both nonlinear Bloch states and gap solitons are represented for fixed number of particles. Gap solitons spread when approaching the energy bands (light-gray shaded regions in the graph), and then become dynamically unstable [18]. Eventually, as happens in the present case at the bottom of the second energy band, they extend to the whole system (or stop existing in an infinite lattice) when entering a band [16]. Overall, the chirality of the system manifests as asymmetric trajectories for positive and negative rotation rates of the lattice. In addition, as we demonstrate next, apparent differences arise in the states belonging to these families, which show distinct density profiles and stability properties.
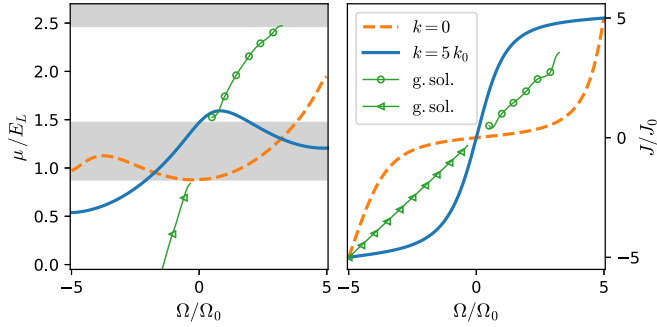
FIG. 2. Trajectories of nonlinear Bloch waves (solid and dashed lines) and gap solitons (thin lines with symbols) in a ring lattice moving with angular rotation Ω. All states contain the same number of particles, so that the varying rotation translates into a varying interaction. Nonlinear Bloch waves are characterized by the wave number k that indexes their quasimomentum, whereas gap soliton trajectories differ for positive (open circles) and negative (open triangles) currents. Left: Energy eigenstates measured in units of the lattice recoil energy E_L; the underlying energy bands of the linear problem (shaded regions) are represented for comparison. Right: Average current density in units of $J_0 = N\Omega_0$.

Figure 3(a) shows the density and phase profiles of two typical gap solitons with the same number of particles and opposite lattice rotation. For positive rotation rate (top panel) the soliton is situated between the first and second energy bands, corresponding to the family represented by lines with open circles in Fig. 2. For negative rotation (bottom panel) the soliton belongs to the family lying in the semi-infinite gap, indicated by lines with open triangles in Fig. 2. The latter soliton, having negative current and then effective attractive interparticle interaction, is comparatively more compact than the former, and occupies just one lattice site. In contrast, as can be seen in Fig. 3(b), the density profiles of two nonlinear Bloch waves with equal quasimomentum $k = 5\,k_0$ but opposite lattice rotations, hence opposite current densities, are almost indistinguishable (notwithstanding, the differences become clearer for increasing number of particles).

D. Linear stability analysis

We have studied the linear stability of the stationary states reported in Fig. 2 by numerically solving the corresponding Bogoliubov equations (5). Before analyzing our results, it is insightful to recall the scenario of equivalent states with contact interparticle interactions; we particularize it for otherwise equal parameters as in Fig. 2. In such a case, while there is no difference regarding the sign of the quasimomentum, the dynamical stability depends strongly on the character of the contact interactions, either repulsive or attractive. For the former case, it is known that Bloch states close to the edge of the Brillouin zone become unstable; how close depends in turn on the strength of the interactions and the lattice depth [20]. The opposite happens for attractive contact interactions, where Bloch states close to zero quasimomentum become unstable; in this latter situation, one can understand the source of instability as associated with smoother, slowly varying density profiles, on which modulation instability can operate due to the existence of lower-energy states with localized density
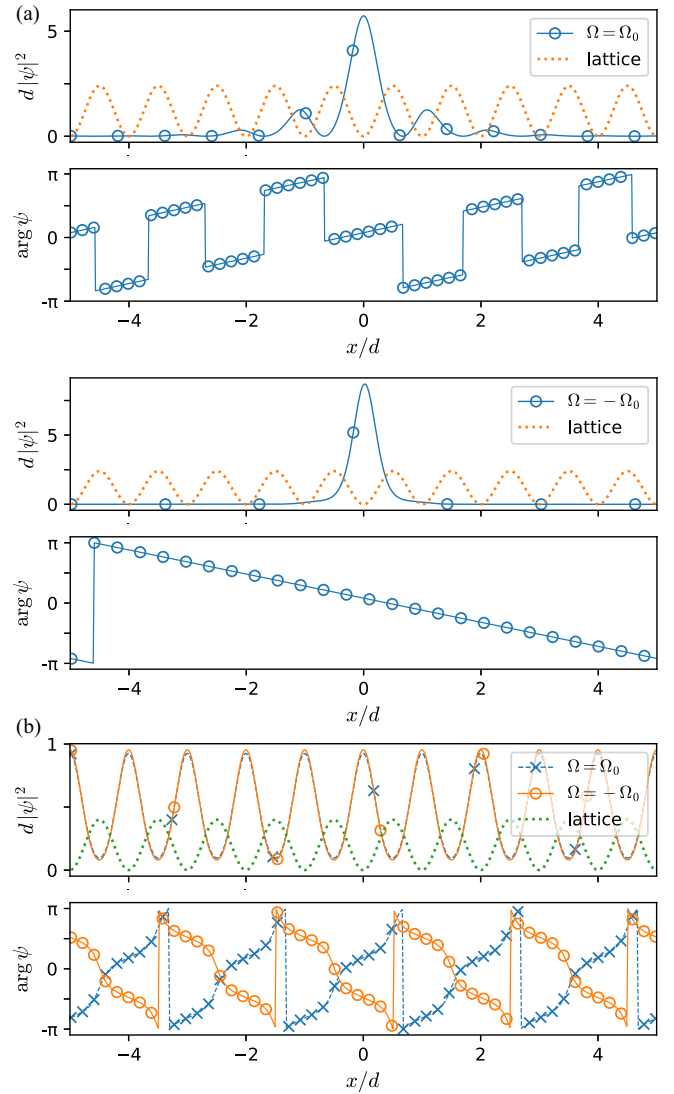

FIG. 3. Gap solitons (a) and nonlinear Bloch waves with quasimomentum $k = 5\,k_0$ (b), for positive $\Omega = \Omega_0$ and negative $\Omega = -\Omega_0$ lattice rotations, and otherwise equal parameters to those used in Fig. 2.

profiles. Regarding fundamental (one main peak) gap solitons, although instabilities can be found when their chemical potential approaches a linear energy band, they are usually stable states.

Our results in current-interacting systems show, in general, a trend similar to the scenario of contact interactions. The main difference resides in the asymmetry between positive and negative quasimomenta, which can be mapped into systems with effective positive and negative contact interactions, respectively. Another particular difference is observed in the stability of gap solitons with positive rotation rates for the lattice depth considered in Fig. 2, $s = 2$, for which we have not found stable cases, despite the fact that the energy of the unstable modes (having complex frequencies) can be very small in comparison with the corresponding energy eigenvalue μ. Still, we did find stability for these solitons at higher values of the lattice depth.
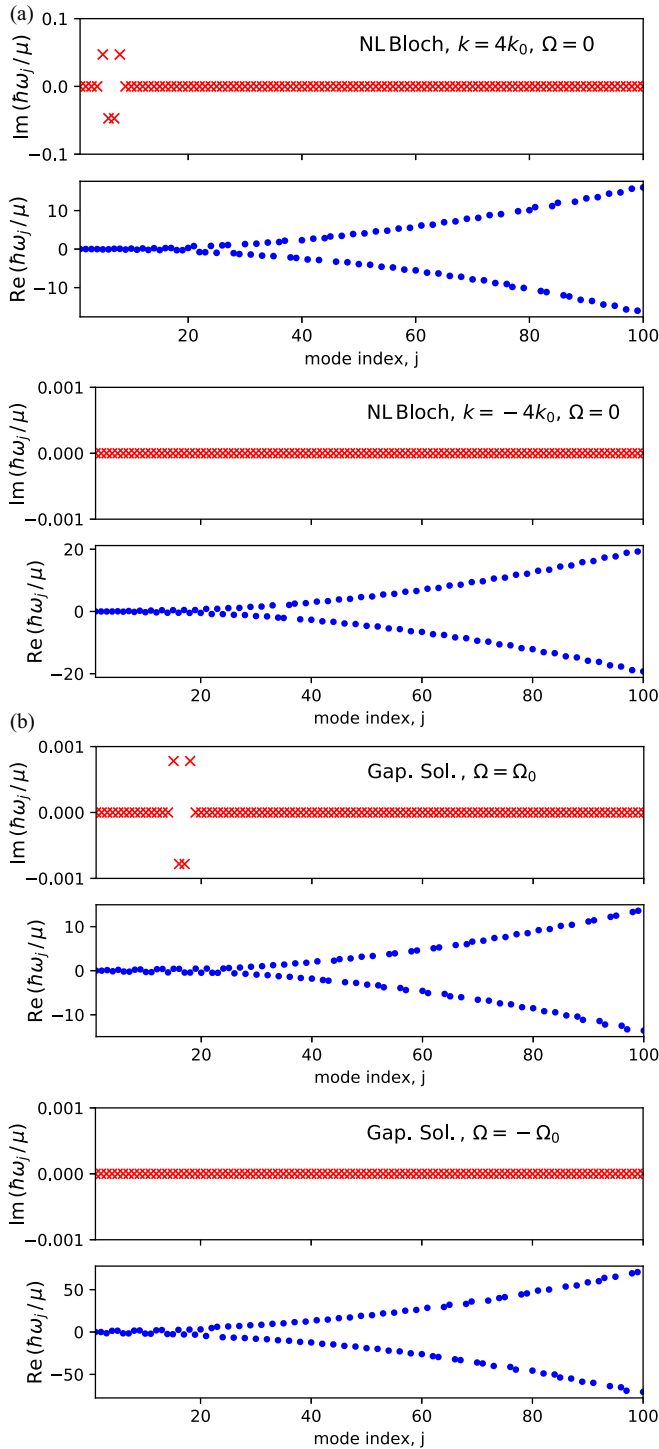
FIG. 4. Linear excitation modes of stationary states for fixed number of particles. (a) Nonlinear Bloch states with $k = 4\,k_0$ in a lattice at rest. (b) Gap solitons with opposite rotation rates shown in Fig. 3.

Several examples of these general features on linear stability are presented in Fig. 4; both the real and imaginary parts of the excitation modes are shown for each state considered. Figure 4(a) shows the excitation energies of two nonlinear Bloch waves with the same absolute value of quasimomentum $|k| = 4k_0$ (close to the edge of the Brillouin zone) in a lattice at

rest $\Omega = 0$. While the state with negative quasimomentum is dynamically stable, the positive-quasimomentum state is not. The scenario is analogous to systems with contact interparticle interactions, hence our results are the opposite (stable for positive rotation and unstable for negative rotation) for states with quasimomentum $|k| = k_0$ (not shown).

Figure 4(b) represents the energy excitations of the two gap solitons shown in Fig. 3. As anticipated, the soliton with negative rotation is dynamically stable, while the soliton with positive rotation, $\Omega = \Omega_0$, presents complex frequencies that can cause the dynamical decay of this stationary state in a real time evolution (see next section). However, for the same parameters but in a deeper lattice, $s = 3$, we have found that the corresponding soliton becomes stable.

IV. DYNAMICS

Despite the linear analysis performed in the previous section, the stability of stationary states can only be ensured through the nonlinear time evolution of the system. To this end, we have solved the time-dependent Eq. (1) for initial stationary states on which perturbative noise has been added. Although our results for the subsequent time evolution are consistent with the predictions of the linear stability analysis, we have also found some interesting cases whose dynamics show features of structural stability (small variations of the stationary state profile that do not break qualitatively its structure) despite the presence of unstable linear modes.

Figure 5(a) depicts three snapshots for selected times ($t = 0$, $T/2$, T) of a time evolution, with total time $T = 25\,md^2/\hbar$, of the linearly unstable soliton of Fig. 3(a) with positive rotation rate. As can be seen, it confirms the linear prediction of instability shown in Fig. 4(b), since it displays the tunneling of particles into nearby lattice sites as time passes. The linear analysis predicts also the instability of the nonlinear Bloch states with $k = 5k_0$ and opposite rotation rates shown in Fig. 3(b), with unstable linear modes of higher energy in the case of positive rotation. However, the time evolution, Fig. 5(b), shows a distinct nonlinear dynamics for them. While the positive rotation Bloch state evolves into a nonsymmetric structure that is highly variable in time, the negative rotation one exhibits a small breathing dynamics that does not alter the geometric shape of the initial state. We have checked that different types of small perturbations lead to the same conclusions, and a similar dynamics is shown for evolution times much longer (up to ten times) than the case shown in Fig. 4(b).

One of the most interesting features of the dynamics in optical lattices is the emergence of Bloch oscillations. This phenomenon has been shown to appear in BECs with contact interparticle interactions when the lattice velocity is slowly ramped up [21,22]. It manifests the periodic nature of the system through the ground-state transit from positive to negative quasimomentum states over the first energy band. As a consequence, the system's average velocity oscillates with respect to the lattice velocity. But differently to linear systems, the nonlinearity introduced by the interactions in BECs can lead to the breakdown of Bloch oscillations, which is associated with the instability of Bloch states close to the edge of the Brillouin zone [20]. In addition, the energy band structure
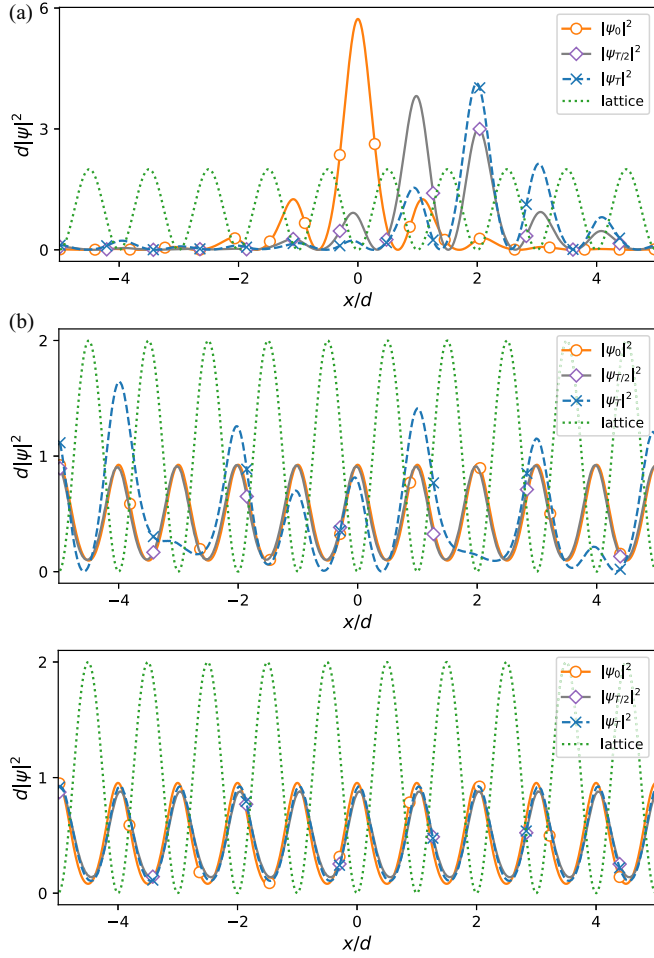
FIG. 5. Selected snapshots of the real time evolution of stationary states shown in Fig. 3 after perturbative noise has been added on the initial states ψ_0. In all the cases, the duration of the total time evolution is $T = 25\, md^2/\hbar$. (a) Gap soliton. (b) Nonlinear Bloch states.
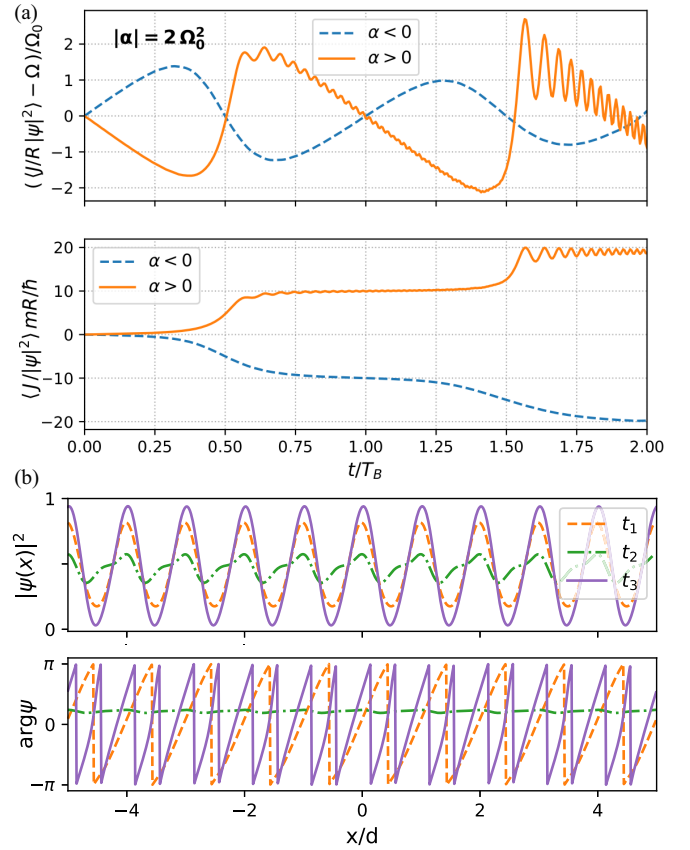

FIG. 6. Bloch oscillations with current-density interactions. (a) Relative angular rotation (top) and linear velocity (bottom) vs time in a lattice with varying rotation rate $\Omega = \alpha t$ for both positive and negative values of the angular acceleration. (b) For $\alpha > 0$, snapshots of the system state at selected times: t_1 at the minimum relative velocity, t_2 at the maximum relative velocity, and t_3 at the first local minimum after the maximum of the relative velocity.

changes with increasing interactions, so that, precisely at the edge of the Brillouin zone, it develops a cusp, first, and a swallow tail configuration, later, that prevents the adiabatic transit between different quasimomentum states [20].

In what follows, we make an exploration of Bloch oscillations in systems with current-dependent interactions. On examination of the dispersion of nonlinear Bloch states for varying rotation, Fig. 2, and despite the lack of symmetry with respect to the rotation direction, one can expect the transit from positive to negative velocities to take place if the states passed across for varying rotation are dynamically stable, or if, these states being unstable, their instability modes grow at slower rate than the transit speed.

The expected period of Bloch oscillations is

$$T_B = \frac{2\pi\hbar}{m\alpha Rd}, \tag{6}$$

where αR is a constant acceleration in the ring, since this is the time taken to cross the first Brillouin zone from quasimomentum $k = -\pi/d$ to π/d. The influence of the nonlinearity on the oscillations in systems with contact interactions

can be captured, at least for smooth density profiles, by effectively modifying the lattice depth as $U_0^{(\text{eff})} = U_0/(1 + 4g_{1D}\bar{n}/E_L)$ [21], where $\bar{n}$ is the average number density. This effective potential provides us with a way to account for the current-density interactions on Bloch oscillations by means of an equivalent effective lattice depth

$$U_0^{(\text{eff})} = U_0\left(1 + 4\frac{\hbar\kappa\bar{J}}{E_L}\right)^{-1}, \tag{7}$$

where $\bar{J}$ is the average current density.

Guided by Eqs. (6) and (7), we have chosen the initial ground state in Fig. 1, with $k = 0$, and have imparted a constant angular acceleration α to the ring lattice. The results are shown in Fig. 6 for the absolute value of the angular acceleration $|\alpha|/\Omega_0^2 = 2$. Figure 6(a) represents the relative rotation of the evolved state with respect to the lattice for negative and positive signs of the acceleration. The observed period of the Bloch oscillations is consistent with Eq. (6), with the zero crossings (or points of zero relative velocity) reached at times t_j that are integer multiples of $T_B/2$, i.e., $t_j = jT_B/2$, and $j = 0, 1, 2, \ldots$. For j odd, the system transits through the edge of the Brillouin zone and the wave function presents

M nodes (associated with the formation of standing waves by Bragg reflections [15]). The latter fact can be interpreted as the presence of M dark solitons caused by the M cores of corresponding vortices in their transition from the outer part to the inner part of the ring [16]. This view is better understood by monitoring the expectation value of the linear velocity measured in ring units $\hbar/mR$, as depicted in the bottom panel of Fig. 6(a). As can be seen, the linear velocity is approximately constant around integer values of t/T_B, that is, around $t_j = l\,T_B$, for $j = 2l$ even, and $l = 0, 1, 2, \ldots$, when the system transits through the center of the Brillouin zone and the velocity takes the value $\sim lM\hbar/mR$, due to $l \times M$ vortices that have entered the inner part of the ring.

Apparent differences can be observed in the smoothness (and also in the duration, see below) of the Bloch oscillations that depend on the sign of the acceleration. Qualitatively, they can be explained by the effective lattice depth of Eq. (7). Since positive (respectively negative) rotations translate into positive (resp. negative) current densities, they decrease (resp. increase) the effective lattice depth and make the lattice progressively less (resp. more) relevant. Contrary to the case of contact interactions, this causes the monotonic variation of the amplitude of Bloch oscillations (the maximum relative speed) after each zero crossing; it keeps increasing (resp. decreasing) for positive (resp. negative) acceleration. For high negative values of the current density the superfluid features of the system tend to disappear, the system state becomes strongly localized, and the current density approaches the lattice rotation, which is reflected in the bottom panel of Fig. 6(a) by a progressively straightened curve, without the marked plateaus of the curve with positive acceleration. On the other hand, the latter adiabatic curve becomes accompanied at higher currents by higher-frequency oscillations, related to Landau-Zener tunneling [21], between configurations with different density modulation [see Fig. 6(b)].

We finish by commenting briefly on the effect of different accelerations. As shown in Fig. 6, for $|\alpha|/\Omega_0^2 = 2$ the decay of Bloch oscillations does not appear before $2T_B$. However, at the lower acceleration of $\alpha = -0.5\Omega_0^2$ (not shown) the oscillations hardly complete one whole period T_B before breaking down, producing the decay of the homogeneous profile over the lattice sites into more localized density peaks. This decay resembles the action of modulation instabilities [23]. Therefore, our results point to the fact that Bloch oscillations that proceed with (still adiabatic, but) higher acceleration last longer, which we attribute to the fact that in this case the unstable modes have a shorter time to grow.

V. CONCLUSIONS

We have reported on gap solitons and nonlinear Bloch states in a rotating ring lattice within a theory with current-density interactions. Our results show that the presence of chirality is manifest in all the states considered, including their spectrum of linear excitations and the display of Bloch oscillations for constant angular acceleration. A novelty is the existence of stationary and dynamically stable nonregular Bloch states characterized by a modulated density profile.

The recent experimental achievement of this theory in Bose-Einstein condensates of ultracold atoms [4] opens the way for the experimental realization of the states and phenomena that we have described. Although currently optical lattice potentials in a ring are experimentally available [24,25], our results are not restricted to this geometry, and can also be realized in one-dimensional linear lattices, as has been routinely done in the presence of contact interatomic interactions [13,14].

Future prospects of our work include the study of fundamental and higher-order soliton states in different energy gaps, and the extension to realistic two- or three-dimensional systems that reach the quasi-1D regime.

[1] L. W. Clark, B. M. Anderson, L. Feng, A. Gaj, K. Levin, and C. Chin, Phys. Rev. Lett. **121**, 030402 (2018).

[2] F. Görg, K. Sandholzer, J. Minguzzi, R. Desbuquois, M. Messer, and T. Esslinger, Nat. Phys. **15**, 1161 (2019).

[3] K.-X. Yao, Z. Zhang, and C. Chin, Nature (London) **602**, 68 (2022).

[4] A. Frölian, C. S. Chisholm, E. Neri, C. R. Cabrera, R. Ramos, A. Celi, and L. Tarruell, Nature (London) **608**, 293 (2022).

[5] U. Aglietti, L. Griguolo, R. Jackiw, S.-Y. Pi, and D. Seminara, Phys. Rev. Lett. **77**, 4406 (1996).

[6] R. Jackiw, J. Nonlinear Math. Phys. **4**, 261 (1997).

[7] M. J. Edmonds, M. Valiente, G. Juzeliūnas, L. Santos, and P. Öhberg, Phys. Rev. Lett. **110**, 085301 (2013).

[8] M. J. Edmonds, M. Valiente, and P. Öhberg, Europhys. Lett. **110**, 36004 (2015).

[9] R. J. Dingwall and P. Öhberg, Phys. Rev. A **99**, 023609 (2019).

[10] I. A. Bhat, S. Sivaprakasam, and B. A. Malomed, Phys. Rev. E **103**, 032206 (2021).

[11] R. J. Dingwall, M. J. Edmonds, J. L. Helm, B. A. Malomed, and P. Öhberg, New J. Phys. **20**, 043004 (2018).

[12] Q. Jia, H. B. Qiu, and A. M. Mateo, Phys. Rev. A **106**, 063314 (2022).

[13] O. Morsch and M. Oberthaler, Rev. Mod. Phys. **78**, 179 (2006).

[14] F. Schäfer, T. Fukuhara, S. Sugawa, Y. Takasu, and Y. Takahashi, Nat. Rev. Phys. **2**, 411 (2020).

[15] C. Kittel and P. McEuen, *Introduction to Solid State Physics* (Wiley, New York, 2018).

[16] A. Muñoz Mateo, V. Delgado, M. Guilleumas, R. Mayol, and J. Brand, Phys. Rev. A **99**, 023630 (2019).

[17] M. Machholm, A. Nicolin, C. J. Pethick, and H. Smith, Phys. Rev. A **69**, 043604 (2004).

[18] P. J. Y. Louis, E. A. Ostrovskaya, C. M. Savage, and Y. S. Kivshar, Phys. Rev. A **67**, 013602 (2003).

[19] M. Krömer, C. Menotti, L. Pitaevskii, and S. Stringari, Eur. Phys. J. D. **27**, 247 (2003).

[20] B. Wu and Q. Niu, New J. Phys. **5**, 104 (2003).

[21] D.-I. Choi and Q. Niu, Phys. Rev. Lett. **82**, 2022 (1999).

[22] O. Morsch, J. H. Müller, M. Cristiani, D. Ciampini, and E. Arimondo, Phys. Rev. Lett. **87**, 140402 (2001).

[23] V. Zakharov and L. Ostrovsky, Physica D **238**, 540 (2009).

[24] M. Sakamoto, K. Oka, R. Morita, and N. Murakami, Opt. Lett. **38**, 3661 (2013).

[25] K. Yamane, M. Sakamoto, N. Murakami, R. Morita, and K. Oka, Opt. Lett. **41**, 4597 (2016).